

Apparent line tension induced by surface-active impurities

Fabio Staniscia and Matej Kanduč*

Jožef Stefan Institute, Jamova 39, 1000 Ljubljana, Slovenia

E-mail: matej.kanduc@ijs.si

Abstract

Line tension in wetting processes is of high scientific and technological relevance, but its understanding remains vague, mainly because of its difficult determination. A widely used method to extract a line tension relies on the variation of a droplet’s contact angle with the droplet’s size. Such an approach yields the apparent line tension, which is an effective parameter that factors in numerous contributions to the finite-size dependence, thus masking the actual line tension in terms of the excess free energy of the three-phase contact line. Based on our recent computer simulation study, we investigate how small amounts of nonionic surfactants, such as surface-active impurities, contribute to the apparent line tension in aqueous droplets. When depositing polydisperse droplets, their different surface-area-to-volume ratios can result in different final bulk concentrations of surfactants, different excess adsorptions to the interfaces, and, consequently, different contact angles. We show that already trace amounts of longer-chained surfactants in a pre-contaminated liquid are enough to affect measurements of the apparent line tension. Our analysis quantifies to what extent “background” impurities, inevitably present in all kinds of experimental settings, limit the resolution of line-tension measurements, which is crucial for avoiding data misinterpretation.

KEYWORDS: *wetting, contact angle, surface tension, line tension, surfactants, impurities*

1. INTRODUCTION

The research of wetting phenomena has a long and rich history, owing to its ubiquity in natural and engineering processes.^{1,2} Its core lies in measurements of contact angles of sessile droplets on solid substrates, which is considered the gold standard in wettability characterization.³ The starting point is provided by the classical Young equation $\cos \theta_0 = (\gamma_{sv} - \gamma_{sw})/\gamma$, which relates the contact angle of a macroscopic droplet, θ_0 , on a partially wettable surface to the surface–vapor (γ_{sv}), surface–water (γ_{sw}), and water–vapor (γ) surface tensions, in the case of water as the liquid. The Young equation, by which the contact angle is independent of the droplet size, has been widely used and confirmed for large, macroscopic droplets. A historically influential extension was introduced by Gibbs,⁴ who postulated the concept of line tension, τ , as the excess free energy per unit length of the three-phase contact line of the droplet. Its implementation leads to the modified Young equation, also termed the Boruvka–Neumann equation^{5,6}

$$\cos \theta = \cos \theta_0 - \frac{\tau}{\gamma a} \quad (1)$$

according to which the contact angle becomes dependent on the droplet’s size. Here, the second term on the right-hand side represents the correction due to the line tension to the macroscopic value, with a being the droplet’s base radius.

The significance of line tension reaches far beyond the contact angles of sessile droplets. Line tension plays a crucial role in heterogeneous nucleation,^{7–10} vaporization,¹¹ droplet spreading and fragmentation,^{12,13} the stability of foams, films, filaments, droplets, and nanobubbles,^{14–19} and even in hydrophobic interactions²⁰ to name but a few. Therefore, understanding line tension is paramount for many phenomena in different scientific and technological fields. The origin of line tension has been studied extensively and attributed

to the imbalance of the intermolecular forces in the three-phase confluence region.^{21–23} Experiments of various liquids and substrates report the span of line tensions over seven orders of magnitude, ranging from 10^{-12} to 10^{-5} N and of either sign.^{24–30} On the contrary, most theoretical studies estimate line tension magnitudes near the lower limit of the experimental range,^{22,31–33} leaving the larger values in experiments poorly understood.

Over time, Eq. 1 has become the standard for determining the line tension from the plots of $\cos \theta$ against the inverse base radius of sessile droplets in experimental and simulation studies.^{11,34–37} Yet, it has become clear that there are additional contributions to $\cos \theta$ in wetting processes that scale inversely with radius and, with that, obscure the “actual” line tension as originally defined by Gibbs. The contributing physical effects can originate from the contact line itself (e.g., line tension stiffness, contact line pinning)^{33,38–41} or from the interface and bulk regions of the droplet and have nothing to do with the three-phase contact line. Examples of those include the curvature-dependent surface tension,^{33,40} pressure-dependent surface tension,^{42–44} gravitational effects (for millimeter-sized droplets),²⁸ and adsorption of surface-active molecules—which is the topic of this paper. Therefore, extracting the line tension from the fit of the modified Young equation (Eq. 1) is today regarded as the *pseudo* or *apparent line tension*—an empirical parameter that lumps together all size-dependent contributions to the contact angle.^{24,28,37,45,46} In that sense, the term is a misnomer as it does not necessarily have to do *only* with the three-phase contact line, but it merely characterizes deviations from the “ideal” Young case. Despite laborious experimental and theoretical efforts in the past decades, line tension remains an elusive quantity up to this day. One of the widely recognized hurdles in contact angle measurements is contamination.^{47,48} It is, unfortunately, difficult to prove that measurements made in aqueous systems are free from impurities. Impurities, ranging from surface-active molecules to insoluble organic

materials, can be present in the liquid, on the substrate, or can come from contaminated air (i.e., airborne contamination).⁴⁹ Airborne hydrocarbons exist almost everywhere, even inside nanofabrication cleanrooms.⁵⁰ For instance, it has been recognized that airborne contamination greatly impacts the wettability of some materials, including silica surfaces,^{51,52} transition-metal semiconductors,^{53,54} and graphene,^{55,56} leading to the long-lasting controversy about its actual contact angle.

Impurities impact wetting in multiple ways, depending on their type. For instance, insoluble impurities that strongly adsorb to the substrate form a static adlayer. Its effect can be tackled, for example, by Lifshitz-based models and density functional theory calculations of optical properties.⁵⁷ On the contrary, if impurities are soluble surface-active molecules, their adsorption to droplet's interfaces modifies the contact angle via the Lucassen-Reynders equation.⁵⁸ In fact, not much attention has been devoted to the processes in which droplets end up with surfactants whose concentration systematically varies with the droplet's size.

In this study, we analyze two common protocols for depositing polydisperse sessile droplets that result in a systematic variation in the internal bulk concentration of surfactants with droplet size. The size variation leads to a size-dependent contact angle and hence engenders a contribution to the apparent line tension. We will demonstrate the outcomes based on the cases of linear alcohols, which provide simple insight into the role that the chain length plays in these processes.

2. ADSORPTION OF SURFACTANTS AND THE CONTACT ANGLE

When surface-active molecules are dissolved in a water droplet, some of them will adsorb to accessible interfaces as schematically shown in Fig. 1. At sufficiently low concentrations, the adsorption is linearly proportional to bulk concentration c , well inside the droplet. Thus, for the adsorption (characterized as the surface excess) to the water–vapor, substrate–water, and substrate–vapor interfaces of the droplet, we write respectively

$$\Gamma_{wv} = K_v c \quad (2)$$

$$\Gamma_{sw} = K_s c \quad (3)$$

$$\Gamma_{sv} = 0 \quad (4)$$

where K_v and K_s are the *adsorption coefficients* to the water–vapor and substrate–water interface, respectively. Here, we assume no adsorption at the bare substrate–vapor interface, which is the case for well-soluble surfactants.⁵⁹

Nonionic organic surfactants are driven to nonpolar interfaces by the hydrophobic effect, owing to their nonpolar tails, typically alkyl chains made up of methyl groups ($-\text{CH}_2-$). We will base our study on linear primary alcohols, in which the hydroxy group ($-\text{OH}$) is bonded to an alkyl chain of a variable length. For brevity, we will term them by the number of carbon atoms (*i.e.*, the chain length) as C1, C2, etc. Such a homologous series of linear alcohols is a simple and very insightful model system to study the surfactant effect based on the chain length.

In Fig. 2 we show adsorption coefficients obtained in our recent molecular dynamics (MD) simulation study⁵⁹ for three short-chained n -alcohols (bulky symbols): methanol (C1), propanol (C3), and pentanol (C5). The results are shown for the water–vapor interface as well as solid substrates with three different contact angles θ_w (tuned by the polarity of the surface groups), featuring a hy-

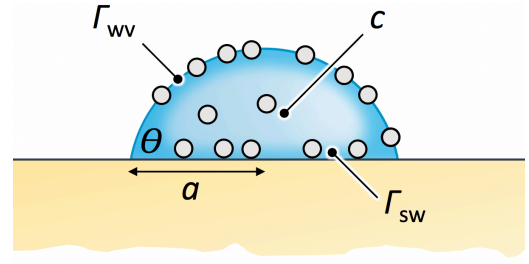


Figure 1: Distribution of surfactants (grey circles) in a sessile droplet of contact angle θ and base radius a : Internal bulk concentration is denoted by c , and adsorptions to the water–vapor and substrate–water interfaces are denoted by Γ_{wv} and Γ_{sw} , respectively.

drophilic surface ($\theta_w = 45^\circ$), intermediate surface ($\theta_w = 97^\circ$), and hydrophobic surface ($\theta_w = 135^\circ$). These contact angles correspond to a pure water droplet without surfactants.

Hydrophobic hydration is known for its volume-to-area scaling crossover with an increasing hydrophobe size.⁶⁰ However, extending the alkyl chain length makes both the volume as well as the surface area increase linearly. Therefore, the transfer free energies scale very well with the number of carbon atoms in their tails,^{59,61} and consequently, the adsorption coefficients scale exponentially with the number of carbon atoms. The simplest mathematical model that captures the behavior of the adsorption coefficients with chain length is thus,

$$K_v = b_v e^{\alpha_v n_c} \quad (5)$$

$$K_s = b_s e^{\alpha_s n_c} \quad (6)$$

where n_c is the number of carbon atoms. The coefficients b_i and α_i are model parameters, which we fit to the simulation data, as shown by the lines in Fig. 2. The fitted exponential trend for the water–vapor interface agrees reasonably well with experimental data extracted from the collection of Bleys and Joos⁶² (blue crosses).

The adsorption of surfactants to both droplet interfaces (Fig. 1) lowers their surface tensions and changes the wetting contact angle. The change can be calculated from the Lucassen-Reynders equation,⁵⁸

$$\frac{d(\gamma \cos \theta)}{d\gamma} = \frac{\Gamma_{sv} - \Gamma_{sw}}{\Gamma_{wv}} \quad (7)$$

Using the adsorption relations given by Eqs. 2–4, leads to (see Appendix A for derivation),

$$\frac{K_v \cos \theta + K_s}{K_v \cos \theta_w + K_s} = \exp\left(\frac{k_B T K_v c}{\gamma}\right) \quad (8)$$

where θ and θ_w refer to the contact angles of a surfactant-laden and pure water droplet, respectively. For small changes in the water contact angle around θ_w , Eq. 8 simplifies into⁵⁹

$$\theta(c) = \theta_w - k_B T \frac{K_v \cos \theta_w + K_s}{\gamma \sin \theta_w} c \quad (9)$$

Surfactants (featuring positive K_v and K_s) mostly cause the contact angle to decrease (which is strictly true for $\theta_w < 90^\circ$).

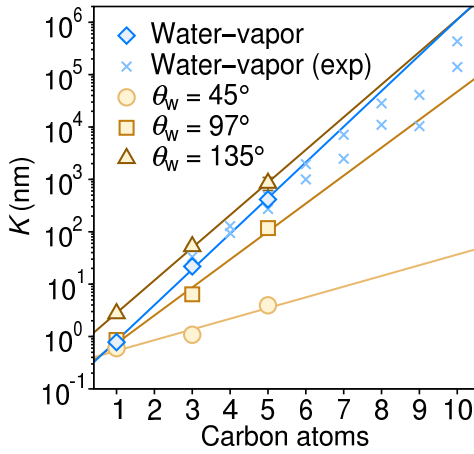


Figure 2: Adsorption coefficients to water–vapor (K_v) and substrate–water interfaces (K_s) with different contact angles θ_w for n -alcohols versus the number of alkyl carbon atoms. The MD simulation data are taken from Ref. 59. For comparison, experimental data for the water–vapor interface taken from Bleys and Joos⁶² are shown by blue crosses. The solid lines are the fits of Eqs. 5 and 6 to the MD data points. The fitting coefficients are $b_v = 0.173$ nm and $\alpha_v = 1.569$ for the water–vapor interface and $b_s = 0.333$ nm, 0.216 nm, 0.674 nm and $\alpha_s = 0.471$ nm, 1.229 nm, 1.434 nm for the substrate–water interfaces with $\theta_w = 45^\circ$, 97° , 135° , respectively.

3. DROPLET DEPOSITION AND CONTACT-ANGLE VARIATION

Based on Eq. 9, the contact angle changes linearly with the surfactant concentration c in the bulk interior of a droplet. Importantly, the change is not directly dependent on the droplet’s size. However, depending on how the droplets get contaminated, the droplet size can influence the internal bulk concentration and, with that, indirectly the contact angle. In this study, we will analyze two routes (named scenarios A and B) in which deposited polydisperse droplets end up with surfactant concentrations that systematically vary with their size. In scenario A, all freshly generated droplets are pre-contaminated by the same total concentration of surfactants and are then deposited on a clean substrate (Fig. 3a). In scenario B, pure water droplets are deposited onto a pre-contaminated substrate (Fig. 3b).

3.1. Scenario A. We first take a closer look at scenario A. As schematized in Fig. 3a, we here consider that all droplets at their formation contain uniformly distributed surfactants of concentration c_0 , also referred to as *total concentration*.

This scenario can be realized, for instance, in the atomization of a contaminated bulk liquid, which is rapidly dispersed into smaller droplets of various sizes (e.g., in the process of spraying and precipitation).^{26,63} Another very relevant protocol is droplet deposition by a syringe or pipette, as commonly used for creating larger droplets. While a droplet is forming at the tip of the syringe, surfactants first have to diffuse to the freshly formed air–water interface from the contaminated bulk interior. It is known that it takes several minutes for typical impurities to adsorb to a fresh air–water interface.⁴⁹ The adsorption time can be estimated as follows. Assuming the adsorption to be a diffusion-controlled process, the time needed

for the formation of the adsorbed layer can be roughly estimated from Sutherland’s solution of the diffusion equation as $\tau \approx K_v^2/D$, where D is the diffusion coefficient of surfactants in water.⁶⁴ This estimate matches the time it takes for surfactants to diffuse over the distance K_v , which corresponds to the slab thickness in the bulk solution that contains the same number of surfactants as adsorbed at the interface in equilibrium. Diffusion coefficients only marginally depend on the chain length for short-chain alcohols and are on the order of $D \sim 1 \text{ nm}^2/\text{ns}$,⁶⁵ whereas the adsorption coefficients vary exponentially with chain length (Eq. 5). With these assumptions, we obtain the estimated adsorption times of around $\tau \sim 0.1$ ms for C5, 1 s for C8, and already 10 min for C10. This means that surfactants longer than around 8 or 9 carbon atoms cannot adsorb to the interface within typical times of droplet formations by a syringe. The syringe technique therefore classifies as scenario A for longer-chain surfactants.

After the contaminated droplets deposit on a clean substrate, the surfactants redistribute by diffusion inside each droplet to reach thermodynamic equilibrium, satisfying Eqs. 2–4 (Fig. 3a). By doing so, the internal bulk concentration in the droplets lowers from c_0 to c . The conservation of the number of surfactants in the droplet after equilibration demands

$$V c_0 = V c + A_{\text{cap}} \Gamma_{\text{vw}} + A_{\text{base}} \Gamma_{\text{sw}} \quad (10)$$

where the three terms on the right-hand side correspond to the total number of surfactants in the droplet’s bulk, at the droplet’s cap, and at its base area, respectively. See Appendix B for the geometrical expressions for the volume and surface areas.

This brings us to the following dependence of the bulk concentration on base radius

$$c = \frac{c_0}{1 + a^*/a} \quad (11)$$

where we have introduced the *partition radius* a^*

$$a^* = 6 \frac{K_v + K_s \cos^2(\theta_w/2)}{\sin \theta_w + \tan(\theta_w/2)} \quad (12)$$

It is not difficult to see from Eq. 11 that the ratio a^*/a equals the ratio between the adsorbed and nonadsorbed surfactants in the droplet, thus, a^* characterizes the length scale of surfactant partitioning.

In short, the variation of the internal concentration (Eq. 11) has its origin in the fact that the surface-area-to-volume ratio varies with the droplet size. The depletion of the surfactants from the bulk is therefore more significant in smaller droplets. For very large droplets, the depletion is small, and the bulk concentration remains unchanged, $c \approx c_0$. The macroscopic contact angle of surfactant-laden droplets is therefore $\theta_0 \equiv \theta(c_0)$. See Fig. 3c for illustration. Using Eq. 9, we compute the change of the contact angle from a macroscopically large droplet $\Delta\theta(c) \equiv \theta(c) - \theta_0$, which is

$$\Delta\theta(c) = k_B T \frac{K_v \cos \theta_w + K_s}{\gamma \sin \theta_w} (c_0 - c) \quad (13)$$

and after expressing it in terms of base radius (using Eq. 11),

$$\Delta\theta(a) = k_B T \frac{K_v \cos \theta_w + K_s}{\gamma \sin \theta_w} \frac{c_0}{1 + a/a^*} \quad (14)$$

Using the above equation, we show in Fig. 4a how the contact angle in scenario A varies as a function of base radius for droplets containing $c_0 = 1$ mM of pentanol (C5) on the three different substrates. As droplets get smaller, the surfactants deplete more from the droplets’ interior, therefore, the contact angles increase. The effect is nonmonotonic in terms of surface hydrophobicity: the vari-

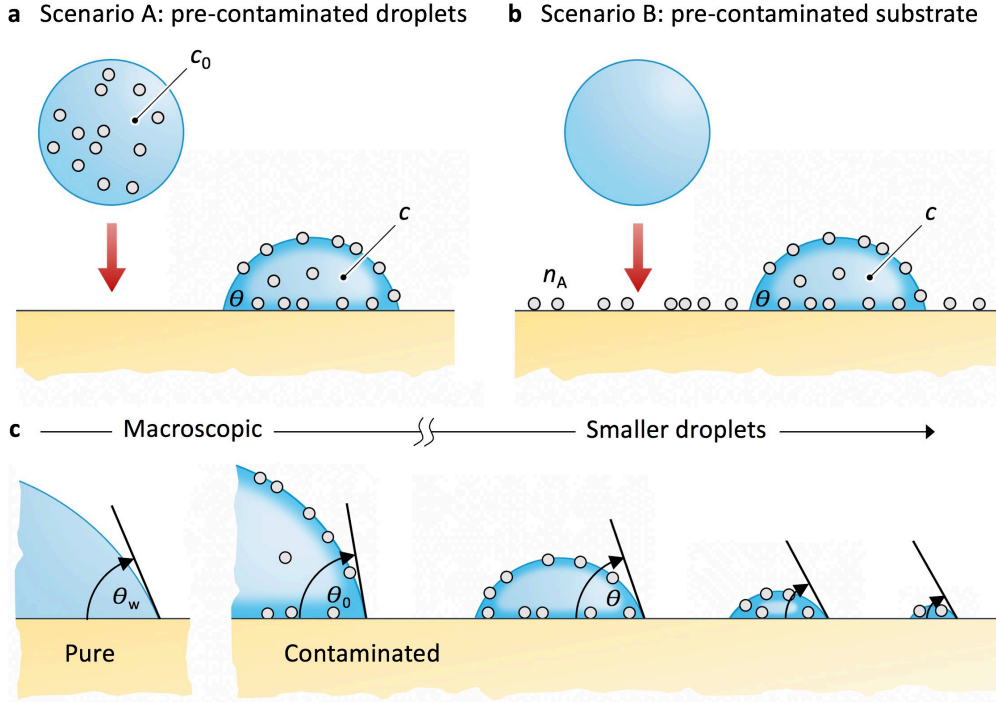


Figure 3: Different scenarios of droplet contamination that lead to size-dependent concentrations of surfactants. (a) Scenario A: Pre-contaminated droplet with uniformly distributed contaminants of the total concentration that is independent of the droplet size. Upon adsorption on a clean substrate, the contaminants redistribute inside the droplet, resulting in a size-dependent bulk concentration c . (b) Scenario B: A pure water droplet deposits on a pre-contaminated substrate with contaminants of areal density n_A . The contaminants hitherto adsorbed in the region of the droplet's base dissolve into the droplet's interior. (c) Variation of the contact angle with droplets' size resulting from dissimilar contaminant concentration. The pure water contact angle is denoted by θ_w and the macroscopic contact angle of a contaminant-laden droplet by θ_0 .

ation is the smallest on the intermediate surface and larger on the hydrophilic and hydrophobic surfaces. This nonmonotonicity in wetting enhancement due to surfactants has been thoroughly investigated elsewhere.⁵⁹

3.2. Scenario B. In scenario B, we consider deposition of pure water droplets on a substrate that is pre-contaminated with surfactants of areal density n_A , as shown in Fig. 3b. After a droplet is deposited, the number of $A_{\text{base}}n_A$ surfactants grasped by the freshly deposited droplet dissolves into the droplet. Let us mention that scenario B could possibly also be relevant to airborne contamination coming from the surrounding atmosphere, where the uptake of contaminants is proportional to the droplet's surface area.

The conservation of surfactants after equilibration in this case demands

$$A_{\text{base}}n_A = Vc + A_{\text{cap}}\Gamma_{\text{vw}} + A_{\text{base}}\Gamma_{\text{sw}} \quad (15)$$

We assume that after the droplet is deposited, no additional surfactants diffuse into the droplet, which is realized by slow enough diffusion of surfactants on the dry substrate, thereby justifying $\Gamma_{\text{sv}} = 0$ (Eq. 4).

In this case, the internal bulk surfactant concentration depends on the droplet's size as

$$c = \frac{\tilde{c}_0}{1 + a/a^*} \quad (16)$$

where the partition radius a^* is again given by Eq. 12. Here, we

have introduced

$$\tilde{c}_0 = \frac{n_A}{K_v/\cos^2(\theta_w/2) + K_s} \quad (17)$$

which corresponds to the maximal internal concentration, reached for small droplets $a \ll a^*$. Contrary to scenario A, very large droplets (with a small surface-to-volume ratio) remain essentially pure, thus the macroscopic contact angle in this case is $\theta_0 = \theta_w$. We again calculate the change of the contact angle from the macroscopic contact angle, $\Delta\theta(c) \equiv \theta(c) - \theta_w$, which is

$$\Delta\theta(a) = -k_B T \frac{K_v \cos \theta_w + K_s}{\gamma \sin \theta_w} \frac{\tilde{c}_0}{1 + a/a^*} \quad (18)$$

This result is similar to scenario A (Eq. 14) but with the opposite sign and \tilde{c}_0 instead of c_0 . In this case, the contact angle grows with increasing size. Because of the similarity in the functional dependence to scenario A, we will not make extra examples for this scenario.

4. APPARENT LINE TENSION

In many experimental as well as simulation studies of sessile droplets, contact angle data are analyzed by plotting $\cos \theta$ against $1/a$. The slope is then used to determine the apparent line tension, as given by Eq. 1. Therefore, we plot the data from Fig. 4a as $\cos \theta - \cos \theta_0$ versus $1/a$ in Fig. 4b. For a better comparison, the data have been shifted by the extrapolated values of $\cos \theta_0$

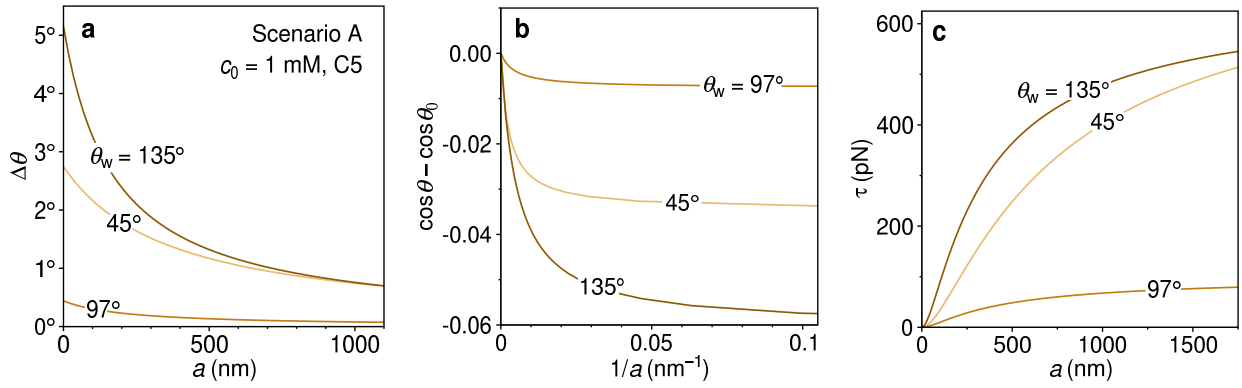


Figure 4: (a) Variation of contact angles of aqueous droplets contaminated with pentanol of total concentration $c_0 = 1$ mM in scenario A on three different substrates as calculated with Eq. 14. (b) Cosine of the contact angle shifted by $\cos \theta_0$ versus $1/a$ of the cases from panel (a). (c) Apparent line tension calculated with Eq. 19.

so that all three cases stem from the same origin. The obtained relation is not linear: the slope is the largest for small a^{-1} , and then starts leveling off with increasing a^{-1} . A nonlinear relation between $\cos \theta$ and $1/a$ is not new and is sometimes experimentally observed,^{23,24} even though approximately linear relations are more commonly reported. Yet, it is important to realize that in typical measurements, droplet radii are varied only within the same order of magnitude.^{23,27,30,34,35,66} Consequently, variations in the slope, even when they exist, are difficult to discern, especially with noisy data. The nonlinear relation does not unequivocally nominate a constant apparent line tension given via Eq. 1. This inspires us to use the differential definition of the apparent line tension,

$$\tau \equiv -\gamma \frac{d \cos \theta}{da^{-1}} \quad (19)$$

The so-obtained apparent line tension is a function of a —it depends on the droplet size. Using Eq. 8 with Eq. 19, we derive the expression for the apparent line tension caused by surfactants in both deposition scenarios as

$$\tau = \frac{\tau_0}{(1 + a^*/a)^2} \quad (20)$$

where we have introduced the asymptotic values

$$\tau_0 = +k_B T a^* (K_v \cos \theta_w + K_s) c_0 \quad (\text{scenario A}) \quad (21)$$

$$\tau_0 = -k_B T a^* (K_v \cos \theta_w + K_s) \tilde{c}_0 \quad (\text{scenario B}) \quad (22)$$

That is, both scenarios are described by the same equations, but with two differences: (i) the opposite sign in τ_0 and (ii) the role of c_0 in scenario A is played by \tilde{c}_0 in scenario B.

In Fig. 4c, we plot the apparent line tensions as calculated from Eqs. 20 and 21 for the cases in Fig 4a and b (1 mM pentanol in scenario A). The apparent line tension starts quadratically increasing with base radius as $\tau_0(a/a^*)^2$ (for $a \ll a^*$) and saturates to τ_0 for large base radius (for $a \gg a^*$).

Let us discuss the consequences of the above results. More important than the absolute value of $\tau(a)$ per se is its relative contribution to measurements of size-dependent contact angles. As suggested by Eq. 1, the importance of the line tension is given by the quantity $\tau/\gamma a$, which is a finite-size correction to $\cos \theta_0$. In general, line tension tends to become more important for smaller droplet sizes, but since, in our case, the apparent line tension scales quadratically with small sizes, its importance is nonmonotonic in size. As demonstrated in Fig 5, the correction $\tau/\gamma a$ is the largest

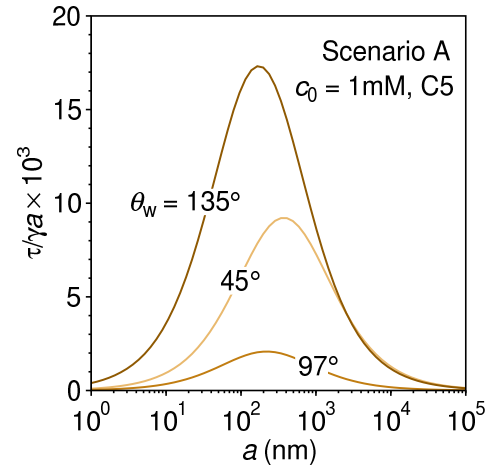


Figure 5: Importance of the apparent line tension to the measurement of $\cos \theta$. Correction to $\cos \theta$ as a function of droplet size for the case of 1 mM pentanol on three different substrates in scenario A.

for intermediate-size droplets and reaches its maximum at $a = a^*$, with the value

$$\left(\frac{\tau}{\gamma a} \right)_{\max} = \frac{\tau_0}{4\gamma a^*} \quad (23)$$

Another significance of the partition radius a^* is that it sets the length scale at which the effect of the apparent line tension due to surfactants is the largest.

5. INFLUENCE OF CHAIN LENGTH

So far, we have quantified the principles by which low concentrations of surface-active molecules induce an apparent line tension in aqueous droplets and exemplified them with pentanol. We now extend the discussion to other surfactants in the context of nonionic impurities characterized by different chain lengths.

To that end, we first take a look at how the chain length influences the partition radius a^* . In Fig. 6a, we show a^* as a function of alkyl-chain length for n -alcohols. The symbols are the values calculated using the adsorption coefficients for the three alcohols from MD

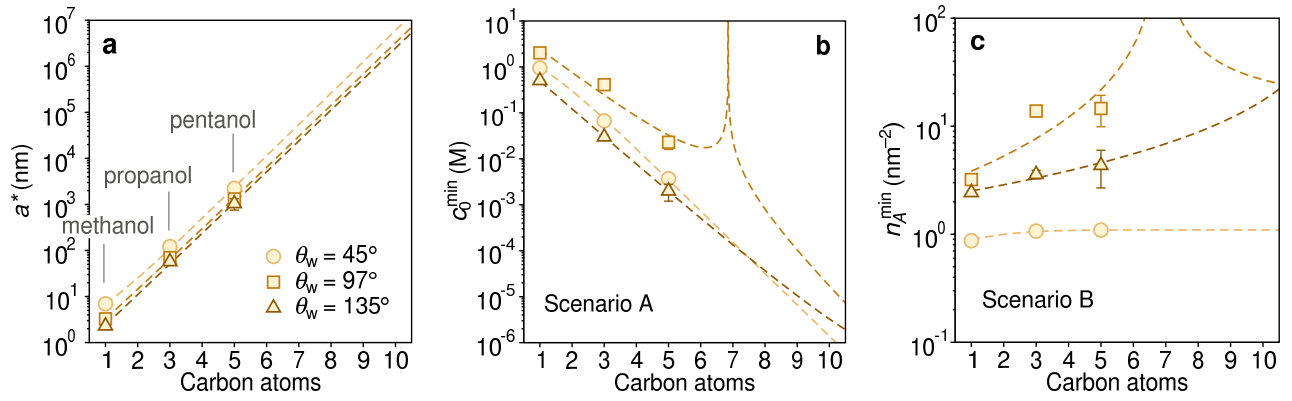


Figure 6: Influence of chain length. (a) Partition radius a^* for linear alcohols as a function of their alkyl chain length. Data are shown for three different substrate contact angles θ_w (the legend applies to all three panels). (b) Minimal bulk concentration that causes a measurable effect in scenario A (Eq. 24). The goniometric uncertainty is chosen as $\delta\theta = 1^\circ$. (c) Minimal areal concentration that causes a measurable effect in scenario B (Eq. 25). The symbols are calculated based on the MD results, and the lines are based on the fitted models for adsorption coefficients (Eqs. 5 and 6).

simulations,⁵⁹ and the dashed lines are calculated using the fitted models (Eqs. 5 and 6). We see that a^* increases approximately exponentially with tail length because a^* is a linear combination of both adsorption coefficients, such that $a^* \sim \max\{K_v, K_s\}$. With each additional carbon atom in the tail, a^* increases approximately by a factor of 4–5. For the C5 alcohol, $a^* \approx 1 \mu\text{m}$, whereas for C10, it reaches macroscopic values of $a^* \approx 1 \text{ mm}$.

The apparent line tension for droplet sizes of $a \approx a^*$ is approximately $\tau(a^*) \approx k_B T K_v^{(s)} c_0 \approx k_B T a^{*2} c_0$ (scenario A), as long as the linear adsorption regime applies. Because of the quadratic dependence on a^* or adsorption coefficients, each additional carbon atom roughly increases the apparent line tension by a factor of ~ 20 for a given total concentration, c_0 . This means that the longer the chain in a surfactant, the lower concentration is needed to cause a detectable contribution to the apparent line tension.

This notion motivates us to pose the question: What is the minimal concentration of surface-active impurities c_0^{min} (scenario A) or n_A^{min} (scenario B) needed to cause a measurable effect in the contact-angle variation? For that, we assume that a goniometric uncertainty in typical contact angle measurements is $\delta\theta = 1^\circ \approx 0.017 \text{ rad}$.^{3,67} We then approximate the minimally measurable difference in cosines in Eq. 1 as $\cos\theta - \cos\theta_w \approx -\sin\theta_w \delta\theta$, which, combined with Eq. 23 where the effect is the largest, gives us the minimal concentration of impurities that causes a measurable effect in scenario A

$$c_0^{\text{min}} = \frac{4\gamma}{k_B T} \frac{\sin\theta_w \delta\theta}{|K_v \cos\theta_w + K_s|} \quad (24)$$

The value of c_0^{min} can be understood as the detectability threshold, above which the presence of surfactants (e.g., undesired impurities) causes a measurable contribution to the apparent line tension as defined by the modified Young equation (Eq. 1).

In Fig. 6b, we plot c_0^{min} for the three substrates in scenario A. First, the threshold concentration decays roughly exponentially with chain length, owing to the fact that $c_0^{\text{min}} \propto 1/\max\{K_v, K_s\}$ (see Eq. 24). The effect is the smallest on the intermediate substrate with $\theta_w \approx 97^\circ$. For the chain length of around $n_C \approx 7$, it happens that $K_v \cos\theta_w + K_s \approx 0$. In this particular case, adsorptions of surfactants to both interfaces cancel each other's contribution to the contact angle, as seen from Eq. 9, and the droplet's contact angle becomes insensitive to the addition of surfactants. The effect of

surfactants is more pronounced on the hydrophobic and hydrophilic substrates, with an order of magnitude lower detectability threshold. For the latter two substrates, the calculated threshold value for methanol is slightly below 1 M; for C3, it is 20 mM, whereas for C5, it is around 1 mM. Based on our mathematical model (dashed line), the trend continues further with a factor of 4–5 decrease for each added carbon to the hydrophobic chain. For C10, it extrapolates down to $c_0^{\text{min}} \approx 10^{-6} \text{ M}$, which corresponds to the total organic carbon (TOC), a non-specific indicator of water quality, of $\sim 100 \mu\text{g/L}$. This value is 1–2 orders of magnitude below TOC values in tap water and comparable to those of some grades of purified water.⁶⁸ For even longer surfactants, we expect that c_0^{min} decreases even further. Such low concentrations pose a serious challenge in ensuring a sufficiently clean environment in experimental measurements. Namely, detecting submicromolar concentrations of surfactant impurities is extremely challenging even with surface-sensitive spectroscopic techniques.^{69,70} The partition radius of C10 is $a^* \approx 1 \text{ mm}$, meaning that its effect is most significant for macroscopically-large droplets. We calculate that the apparent line tension for $1 \mu\text{M}$ of C10 is $\tau_0 \approx k_B T a^{*2} c_0 \approx 10^{-5} \text{ N}$. Such high values lie in the top part of the spectrum of reported values in the literature for line tensions, which are also the least understood. This does not mean, however, that the explanation for such high values lies exclusively in impurities but rather that impurities can be a contributing factor in some cases.

The outcomes of the homologous series of n -alcohols, used as model surfactants in this study, are transferable to other alkyl-based surfactants. Many everyday detergents used in industrial and commercial cleaning formulations have alkyl tails of lengths 10 carbons and above. Impurities may consist of a broad mixture of different species that most likely varies from experiment to experiment. Their contributions could sum up, and polydispersity in the chain length could probably broaden the influential length scale (Fig. 5), leading to a less size-dependent apparent line tension.

Similar to scenario A, we estimate the minimal areal concentration n_A^{min} of surfactants on a pre-contaminated substrate in scenario B that causes a detectable effect in the contact angle variation. This can be easily derived by replacing c_0 in Eq. 24 by \tilde{c}_0 (given by

Eq. 17), which gives us

$$n_A^{\min} = \frac{4\gamma}{k_B T} \left(\frac{K_v / \cos^2(\theta_w/2) + K_s}{K_v \cos \theta_w + K_s} \right) \sin \theta_w \delta \theta \quad (25)$$

As we show in Fig. 6c, the size of the molecule plays a much less important role in scenario B than in scenario A. Here, the adsorption coefficients enter the numerator and the denominator, consequently, the expression in the parentheses is of the order of unity, and the expression becomes almost independent of the surfactant type. This is in stark contrast to scenario A, where the surfactant type plays the utmost important role. Thus, in scenario B, the threshold values of $n_A = 1\text{--}10 \text{ nm}^{-2}$ suggest that nearly the entire surface has to be covered by molecules to cause a measurable effect on apparent line tension. Such circumstances can readily occur when performing experiments in environmental air, especially in urban areas, because of airborne contamination with various hydrocarbons that quickly cover up the whole surface area.^{50,55,56}

Our analysis is based on linear Henry's regime of adsorption, which is valid for small enough concentrations. In Appendix C, we estimate that the range of validity of the linear regime and the subsequent line-tension analysis reaches not far from the detectability threshold. It should be therefore kept in mind that the analysis cannot be quantitatively used for too high surfactant concentrations.

In the end, comparing the outcomes of both scenarios (Figs. 6b and 6c), it appears that trace amounts of pre-existing impurities in the bulk liquid (scenario A) pose a greater challenge to line tension measurements than the contamination of droplets from pre-contaminated surfaces (scenario B). In the latter case, a cleansed or freshly prepared surface in a clean atmosphere can considerably reduce contamination via this route.

6. CONCLUSIONS

This study points to the importance of trace amounts of surface-active impurities in measurements of line tension. We have shown that even tiny amounts of surfactants in deposited aqueous droplets can lead to a notable variation of the contact angles with the droplet's size. A direct consequence is that they contribute to the apparent line tension as traditionally obtained from contact angle measurements of droplets of different sizes. We have quantified the phenomenon for a homologous series of *n*-alcohols as a model system for non-ionic surfactants and got a good insight into how the effect scales with the alkyl-tail length. For longer-tail surfactants, consisting of around 10 carbon atoms and above, already micromolar or submicromolar concentrations cause a measurable effect on the apparent line tension, which can be as large as 10^{-5} N.

Such low concentrations highlight the importance of purity in experimental measurements with the aim of reducing contamination. Despite the care taken in the cleanness of lab equipment and using purified water subjected to sophisticated purification techniques, some residual impurities stemming from various sources are unavoidable^{49,71} and are even challenging to detect.^{69,70} Therefore, it is essential to realize that these "background" impurities limit the experimental resolution of line-tension measurements and, with that, avoid data misinterpretation. Impurities are thus one of several known factors that can contribute to the measurements of the apparent line tension, but, to the best of our knowledge, hitherto not critically considered as a source of possible artifacts.

It is important to mention that our model was intentionally kept minimal and simple to demonstrate the effect. However, impurities can consist of a broad mixture of different species of different tails

and polar-group characters that vary from experiment to experiment. Another viable phenomenon of surfactants is that they can adsorb to the three-phase contact line and, by that, modify the actual line tension directly in the same way as surface adsorption leads to a reduction of the surface tension.⁷² Note that our analysis is based on nonionic surfactants. In contrast, ionic surfactants impose a collective electrostatic interplay with counterions and coions, resulting in a more complex and nonlinear adsorption behavior.⁷³ These effects, not in the scope of the present paper, are interesting points for future research. We studied the surfactant effect in water droplets, but qualitatively similar results we expect for other polar liquids with high surface tensions, whereas liquids with lower surface tensions are expected to be less affected by impurities.

In general, trace amounts of surface-active impurities in aqueous solutions often have a negligible effect on bulk properties but can, in some cases, impact the surface behavior enormously. Some other known interface phenomena in which tiny amounts of impurities play visible roles are the Jones-Ray effect,^{69,70,73} negative zeta potentials of hydrophobic surfaces,⁷⁴⁻⁷⁷ anomalous nanobubble stability,^{78,79} and some dynamical effects at air-water interfaces.⁸⁰⁻⁸²

A. CHANGE IN CONTACT ANGLE

Here we derive Eq. 8, which gives the change in the contact angle due to surfactants. Inserting Eqs. 2-4 into Eq. 7 and performing the derivation of the left-hand side leads to

$$\cos \theta - \gamma \sin \theta \frac{d\theta}{dc} \frac{dc}{d\gamma} = -\frac{K_s}{K_v} \quad (26)$$

We have used the chain rule to express the derivative of θ with respect to bulk concentration c . Next, the water-vapor surface tension in the linear adsorption regime changes with adsorption as $d\gamma = -k_B T d\Gamma_{wv}$, which further leads to $d\gamma/dc = -k_B T K_v$. Inserting the last expression into Eq. 26 and after some rearrangement, we obtain

$$\frac{\gamma \sin \theta d\theta}{K_v \cos \theta + K_s} = -k_B T dc \quad (27)$$

After the integration from θ_w to θ and 0 to c of the left- and right-hand side, respectively, we get

$$\frac{\gamma}{K_v} \ln \frac{K_v \cos \theta + K_s}{K_v \cos \theta_w + K_s} = k_B T c \quad (28)$$

Another small rearrangement gives Eq. 8.

B. SPHERICAL CAP GEOMETRY

A sessile droplet deposited on a solid flat substrate assumes the form of a spherical cap with the contact angle θ and base radius a . Its volume is then

$$V = \frac{\pi a^3}{3} \frac{(2 + \cos \theta) \sin \theta}{(1 + \cos \theta)^2} \quad (29)$$

the water-vapor surface area (the cap) is

$$A_{\text{cap}} = \frac{2\pi a^2}{1 + \cos \theta} \quad (30)$$

and the surface area of its base is

$$A_{\text{base}} = \pi a^2 \quad (31)$$

C. REGIME OF VALIDITY

The bottleneck of the linear adsorption regime (Eqs. 2 and 3) is that long-tailed surfactants could considerably interact with each other already at relatively low adsorption densities. The onset of these interactions can be estimated on the second-order virial expansion level, which gives the surface-tension decrement as⁵⁹

$$\Delta\gamma = -k_{\text{B}}TK_{\text{V}}c + k_{\text{B}}TB_2K_{\text{V}}^2c^2 \quad (32)$$

Here, B_2 is the two-dimensional second virial coefficient of surfactants at the interface. The interaction between surfactants at an interface depends on the balance between the hydrophilic and hydrophobic groups and can be best explored from surface-pressure isotherms. For surfactants that sterically repel, B_2 is positive and roughly equal to the surfactant's cross-section area, $B_2 \simeq A_{\text{surf}}$.

Based on Eq. 32, this defines the range of the linear regime as $c_0^{\text{lin}} = (K_{\text{V}}A_{\text{m}})^{-1}$. The order of magnitude of the ratio between c_0^{min} (Eq. 24) and c_0^{lin} , assuming $|K_{\text{V}} \cos \theta_{\text{w}} + K_{\text{s}}| \sim K_{\text{V}}$ and $\sin \theta_{\text{w}} \sim 1$, is

$$\frac{c_0^{\text{min}}}{c_0^{\text{lin}}} \sim \frac{\gamma A_{\text{m}}}{k_{\text{B}}T} \delta\theta \quad (33)$$

which for $A_{\text{surf}} \sim 0.2\text{--}1.0 \text{ nm}^2$ gives $c_0^{\text{min}}/c_0^{\text{lin}} \approx 0.05\text{--}0.2$. Hence, the detectability threshold lies within the linear regime.

On the contrary, for attractive surfactants that tend to cluster, B_2 can be large and negative, such that the linearity can break down already at lower concentrations. As seen from eq 32, the surface tension is reduced more for attractive surfactants (featuring $B_2 < 0$) at a given concentration compared to repulsive surfactants (featuring $B_2 > 0$). From this, we qualitatively conclude that strongly attractive surfactants impose an even more substantial influence on the apparent line tension.

A similar estimate can be done for scenario B and repulsive surfactants. Assuming $|K_{\text{V}}/\cos^2(\theta_{\text{w}}/2) + K_{\text{s}}| \sim K_{\text{V}}$, we obtain

$$n_{\text{A}}^{\text{lin}} \approx \frac{2}{A_{\text{surf}}} \quad (34)$$

which for $A_{\text{surf}} \sim 0.2\text{--}1.0 \text{ nm}^2$ gives $n_{\text{A}}^{\text{lin}} \approx 2\text{--}10 \text{ nm}^{-2}$, which is right at the crossover of the linear regime.

ACKNOWLEDGMENTS

We acknowledge financial support from the Slovenian Research Agency (contracts P1-0055 and J1-1701).

CONFLICT OF INTEREST

The authors have no conflicts to disclose.

AUTHOR CONTRIBUTIONS

Fabio Staniscia: Formal analysis (supporting); Investigation (equal); Writing – original draft (supporting). **Matej Kanduč:** Conceptualization (lead); Formal analysis (lead); Investigation (equal); Funding acquisition (lead); Visualization (lead); Writing – original draft (lead).

References

- (1) De Gennes, P.-G. Wetting: statics and dynamics. *Rev. Mod. Phys.* **1985**, *57*, 827.
- (2) Bonn, D.; Eggers, J.; Indekeu, J.; Meunier, J.; Rolley, E. Wetting and Spreading. *Rev. Mod. Phys.* **2009**, *81*, 739–805.
- (3) Liu, K.; Vuckovac, M.; Latikka, M.; Huhtamäki, T.; Ras, R. H. Improving surface-wetting characterization. *Science* **2019**, *363*, 1147–1148.
- (4) *The Collected Works of J. Willard Gibbs*; Yale University Press, London, 1957.
- (5) Boruvka, L.; Neumann, A. Generalization of the classical theory of capillarity. *J. Chem. Phys.* **1977**, *66*, 5464–5476.
- (6) Gaydos, J.; Neumann, A. The dependence of contact angles on drop size and line tension. *J. Colloid Interface Sci.* **1987**, *120*, 76–86.
- (7) Joanny, J.; De Gennes, P. Role of long-range forces in heterogeneous nucleation. *J. Colloid Interface Sci.* **1986**, *111*, 94–101.
- (8) Law, B. M. Theory of nucleated wetting. *Phys. Rev. Lett.* **1994**, *72*, 1698.
- (9) Retter, U.; Siegler, K.; Vollhardt, D. Determination of the Nucleus-to-Surroundings Interfacial Tensions and the Line Tension of Lenticular Nuclei Formed from Insoluble Monolayers at the Air-Water Interface. *Langmuir* **1996**, *12*, 3976–3979.
- (10) Lefevre, B.; Saugey, A.; Barrat, J.-L.; Bocquet, L.; Charlaix, E.; Gobin, P.-F.; Vigier, G. Intrusion and extrusion of water in hydrophobic mesopores. *J. Chem. Phys.* **2004**, *120*, 4927–4938.
- (11) Zhang, J.; Leroy, F.; Müller-Plathe, F. Influence of contact-line curvature on the evaporation of nanodroplets from solid substrates. *Phys. Rev. Lett.* **2014**, *113*, 046101.
- (12) Fan, H. Liquid droplet spreading with line tension effect. *J. Condens. Matter Phys.* **2006**, *18*, 4481.
- (13) Paneru, G.; Law, B. M.; Ibi, K.; Ushijima, B.; Flanders, B. N.; Aratono, M.; Matsubara, H. Liquid Droplet Coalescence and Fragmentation at the Aqueous–Air Surface. *Langmuir* **2015**, *31*, 132–139.
- (14) Aronson, A.; Bergeron, V.; Fagan, M. E.; Radke, C. The influence of disjoining pressure on foam stability and flow in porous media. *Colloids Surf. A Physicochem. Eng. Asp.* **1994**, *83*, 109–120.
- (15) Rosso, R.; Virga, E. G. Sign of line tension in liquid bridge stability. *Phys. Rev. E* **2004**, *70*, 031603.
- (16) Brinkmann, M.; Kierfeld, J.; Lipowsky, R. Stability of liquid channels or filaments in the presence of line tension. *J. Condens. Matter Phys.* **2005**, *17*, 2349.
- (17) Guzzardi, L.; Rosso, R.; Virga, E. G. Residual stability of sessile droplets with negative line tension. *Phys. Rev. E* **2006**, *73*, 021602.
- (18) Mechkov, S.; Oshanin, G.; Rauscher, M.; Brinkmann, M.; Cazabat, A.; Dietrich, S. Contact line stability of ridges and drops. *EPL* **2007**, *80*, 66002.
- (19) Guillelot, L.; Biben, T.; Galarneau, A.; Vigier, G.; Charlaix, É. Activated drying in hydrophobic nanopores and the line tension of water. *Proc. Natl. Acad. Sci. U.S.A.* **2012**, *109*, 19557–19562.
- (20) Sharma, S.; Debenedetti, P. G. Evaporation rate of water in hydrophobic confinement. *Proc. Natl. Acad. Sci. U.S.A.* **2012**, *109*, 4365–4370.
- (21) Indekeu, J. Line tension at wetting. *Int. J. Mod. Phys. B* **1994**, *8*, 309–345.
- (22) Amirfazli, A.; Neumann, A. Status of the three-phase line tension: a review. *Adv. Colloid Interface Sci.* **2004**, *110*, 121–141.
- (23) Heim, L.-O.; Bonaccorso, E. Measurement of line tension on droplets in the submicrometer range. *Langmuir* **2013**, *29*, 14147–14153.
- (24) Drelich, J.; Miller, J. D. The line/pseudo-line tension in three-phase systems. *Part. Sci. Technol.* **1992**, *10*, 1–20.
- (25) Duncan, D.; Li, D.; Gaydos, J.; Neumann, A. Correlation of line tension and solid-liquid interfacial tension from the measurement of drop size dependence of contact angles. *J. Colloid Interface Sci.* **1995**, *169*, 256–261.
- (26) Pompe, T.; Herminghaus, S. Three-phase contact line energetics from nanoscale liquid surface topographies. *Phys. Rev. Lett.* **2000**, *85*, 1930.
- (27) Leelamanie, D. A.; Karube, J. Drop size dependence of soil-water contact angle in relation to the droplet geometry and line tension. *Soil Sci. Plant Nutr.* **2012**, *58*, 675–683.
- (28) Law, B. M.; McBride, S. P.; Wang, J. Y.; Wi, H. S.; Paneru, G.; Betelu, S.; Ushijima, B.; Takata, Y.; Flanders, B.; Bresme, F.; Matsubara, H.; Takiue, T.; Aratono, M. Line tension and its influence on droplets and particles at surfaces. *Prog. Surf. Sci.* **2017**, *92*, 1–39.

- (29) Matsubara, H.; Otsuka, J.; Law, B. M. Finite-Size and Solvent Dependent Line Tension Effects for Nanoparticles at the Air–Liquid Surface. *Langmuir* **2018**, *34*, 331–340.
- (30) Zhao, B.; Luo, S.; Bonaccorso, E.; Auernhammer, G. K.; Deng, X.; Li, Z.; Chen, L. Resolving the apparent line tension of sessile droplets and understanding its sign change at a critical wetting angle. *Phys. Rev. Lett.* **2019**, *123*, 094501.
- (31) Indekeu, J. Line tension near the wetting transition: results from an interface displacement model. *Phys. A: Stat. Mech. Appl.* **1992**, *183*, 439–461.
- (32) Getta, T.; Dietrich, S. Line tension between fluid phases and a substrate. *Phys. Rev. E* **1998**, *57*, 655.
- (33) Schimmele, L.; Napiórkowski, M.; Dietrich, S. Conceptual aspects of line tensions. *J. Chem. Phys.* **2007**, *127*, 164715.
- (34) Wang, J.; Betelu, S.; Law, B. Line tension effects near first-order wetting transitions. *Phys. Rev. Lett.* **1999**, *83*, 3677.
- (35) Berg, J. K.; Weber, C. M.; Riegler, H. Impact of negative line tension on the shape of nanometer-size sessile droplets. *Phys. Rev. Lett.* **2010**, *105*, 076103.
- (36) Werder, T.; Walther, J. H.; Jaffe, R.; Halicioglu, T.; Koumoutsakos, P. On the water–carbon interaction for use in molecular dynamics simulations of graphite and carbon nanotubes. *J. Phys. Chem. B* **2003**, *107*, 1345–1352.
- (37) Zhang, J.; Wang, P.; Borg, M. K.; Reese, J. M.; Wen, D. A critical assessment of the line tension determined by the modified Young’s equation. *Phys. Fluids* **2018**, *30*, 082003.
- (38) Marmur, A.; Krasovitski, B. Line tension on curved surfaces: Liquid drops on solid micro-and nanospheres. *Langmuir* **2002**, *18*, 8919–8923.
- (39) Rusanov, A.; Shchekin, A.; Tatyankov, D. The line tension and the generalized Young equation: the choice of dividing surface. *Colloids Surf. A Physicochem. Eng. Asp.* **2004**, *250*, 263–268.
- (40) Kanduč, M. Going Beyond the Standard Line Tension: Size-Dependent Contact Angles of Water Nanodroplets. *J. Chem. Phys.* **2017**, *147*, 174701.
- (41) Zhang, H.; Chen, S.; Guo, Z.; Liu, Y.; Bresme, F.; Zhang, X. Contact line pinning effects influence determination of the line tension of droplets adsorbed on substrates. *J. Phys. Chem. C* **2018**, *122*, 17184–17189.
- (42) Ward, C.; Wu, J. Effect of contact line curvature on solid-fluid surface tensions without line tension. *Phys. Rev. Lett.* **2008**, *100*, 256103.
- (43) Schimmele, L.; Dietrich, S. Line tension and the shape of nanodroplets. *Eur. Phys. J. E* **2009**, *30*, 427–430.
- (44) Tatyankov, D. V.; Shchekin, A. K. Comparable effects of adsorption and line tension on contact angle of a nucleated droplet on a partially wettable substrate. *Interfacial Phenom. Heat Transf.* **2017**, *5*.
- (45) Kanduč, M.; Eixeres, L.; Liese, S.; Netz, R. R. Generalized line tension of water nanodroplets. *Phys. Rev. E* **2018**, *98*, 032804.
- (46) Iwamatsu, M. A generalized Young’s equation to bridge a gap between the experimentally measured and the theoretically calculated line tensions. *J. Adhes. Sci. Technol.* **2018**, *32*, 2305–2319.
- (47) Chang, C.-H.; Franses, E. I. Adsorption dynamics of surfactants at the air/water interface: a critical review of mathematical models, data, and mechanisms. *Colloids Surf., A* **1995**, *100*, 1–45.
- (48) An, H.; Liu, G.; Craig, V. S. Wetting of Nanophases: Nanobubbles, Nanodroplets and Micropancakes on Hydrophobic Surfaces. *Adv. Colloid Interface Sci.* **2015**, *222*, 9–17.
- (49) Ponce-Torres, A.; Vega, E. The effects of ambient impurities on the surface tension. EPJ Web Conf. 2016; p 02098.
- (50) Smith, P. J.; Lindley, P. M. Analysis of organic contamination in semiconductor processing. AIP Conf. Proc. 1998; pp 133–139.
- (51) Iglauer, S.; Salamah, A.; Sarmadivaleh, M.; Liu, K.; Phan, C. Contamination of silica surfaces: Impact on water–CO₂–quartz and glass contact angle measurements. *Int. J. Greenh. Gas Control.* **2014**, *22*, 325–328.
- (52) Saraji, S.; Piri, M.; Goual, L. The effects of SO₂ contamination, brine salinity, pressure, and temperature on dynamic contact angles and interfacial tension of supercritical CO₂/brine/quartz systems. *Int. J. Greenh. Gas Control.* **2014**, *28*, 147–155.
- (53) Chow, P. K.; Singh, E.; Viana, B. C.; Gao, J.; Luo, J.; Li, J.; Lin, Z.; Elías, A. L.; Shi, Y.; Wang, Z.; Terrones, M.; Koratkar, N. Wetting of mono and few-layered WS₂ and MoS₂ films supported on Si/SiO₂ substrates. *ACS nano* **2015**, *9*, 3023–3031.
- (54) Gurarlan, A.; Jiao, S.; Li, T.-D.; Li, G.; Yu, Y.; Gao, Y.; Riedo, E.; Xu, Z.; Cao, L. Van der Waals force isolation of monolayer MoS₂. *Adv. Mater.* **2016**, *28*, 10055–10060.
- (55) Li, Z.; Wang, Y.; Kozbial, A.; Shenoy, G.; Zhou, F.; McGinley, R.; Ireland, P.; Morganstein, B.; Kunkel, A.; Surwade, S. P.; Li, L.; Liu, H. Effect of airborne contaminants on the wettability of supported graphene and graphite. *Nat. Mater.* **2013**, *12*, 925–931.
- (56) Kozbial, A.; Li, Z.; Sun, J.; Gong, X.; Zhou, F.; Wang, Y.; Xu, H.; Liu, H.; Li, L. Understanding the intrinsic water wettability of graphite. *Carbon* **2014**, *74*, 218–225.
- (57) Zhou, Y.; Reed, E. J. Microscopic origins of the variability of water contact angle with adsorbed contaminants on layered materials. *J. Phys. Chem. C* **2018**, *122*, 18520–18527.
- (58) Lucassen-Reynders, E. Contact Angles and Adsorption on Solids. *J. Phys. Chem.* **1963**, *67*, 969–972.
- (59) Staniscia, F.; Guzman, H. V.; Kanduč, M. Tuning Contact Angles of Aqueous Droplets on Hydrophilic and Hydrophobic Surfaces by Surfactants. *J. Phys. Chem. B* **2022**, *126*, 3374–3384.
- (60) Chandler, D. Interfaces and the driving force of hydrophobic assembly. *Nature* **2005**, *437*, 640–647.
- (61) Singh, H.; Sharma, S. Hydration of Linear Alkanes is Governed by the Small Length-Scale Hydrophobic Effect. *J. Chem. Theory Comput.* **2022**.
- (62) Bleys, G.; Joos, P. Adsorption kinetics of bolaform surfactants at the air/water interface. *J. Phys. Chem.* **1985**, *89*, 1027–1032.
- (63) Wang, R.; Cong, L.; Kido, M. Evaluation of the wettability of metal surfaces by micro-pure water by means of atomic force microscopy. *Appl. Surf. Sci.* **2002**, *191*, 74–84.
- (64) Sutherland, K. The kinetics of adsorption at liquid surfaces. *Aust. J. Chem.* **1952**, *5*, 683–696.
- (65) Hao, L.; Leaist, D. G. Binary mutual diffusion coefficients of aqueous alcohols. Methanol to 1-heptanol. *J. Chem. Eng. Data* **1996**, *41*, 210–213.
- (66) McBride, S. P.; Law, B. M. Influence of line tension on spherical colloidal particles at liquid-vapor interfaces. *Phys. Rev. Lett.* **2012**, *109*, 196101.
- (67) Vuckovac, M.; Latikka, M.; Liu, K.; Huhtamäki, T.; Ras, R. H. Uncertainties in contact angle goniometry. *Soft Matter* **2019**, *15*, 7089–7096.
- (68) Zhang, X.; Yang, Y.; Ngo, H. H.; Guo, W.; Wen, H.; Wang, X.; Zhang, J.; Long, T. A critical review on challenges and trend of ultra-pure water production process. *Sci. Total Environ.* **2021**, *785*, 147254.
- (69) Duignan, T. T.; Peng, M.; Nguyen, A. V.; Zhao, X.; Baer, M. D.; Mundy, C. J. Detecting the undetectable: The role of trace surfactant in the Jones-Ray effect. *J. Chem. Phys.* **2018**, *149*, 194702.
- (70) Peng, M.; Duignan, T. T.; Nguyen, C. V.; Nguyen, A. V. From Surface Tension to Molecular Distribution: Modeling Surfactant Adsorption at the Air–Water Interface. *Langmuir* **2021**, *37*, 2237–2255.
- (71) Persson, C. M.; Claesson, P. M.; Lunkenheimer, K. Interfacial behavior of n-decyl-β-D-maltopyranoside on hydrophobic interfaces and the effect of small amounts of surface-active impurities. *J. Colloid Interface Sci.* **2002**, *251*, 182–192.
- (72) Widom, B. Adsorption at a line of three-phase contact. *Colloids Surf. A Physicochem. Eng. Asp.* **2004**, *239*, 141–144.
- (73) Uematsu, Y.; Bonthuis, D. J.; Netz, R. R. Charged surface-active impurities at nanomolar concentration induce Jones-Ray effect. *J. Phys. Chem. Lett.* **2018**, *9*, 189–193.
- (74) Zimmermann, R.; Dukhin, S.; Werner, C. Electrokinetic measurements reveal interfacial charge at polymer films caused by simple electrolyte ions. *J. Phys. Chem. B* **2001**, *105*, 8544–8549.
- (75) Roger, K.; Cabane, B. Why are hydrophobic/water interfaces negatively charged? *Angew. Chem. Int. Ed.* **2012**, *51*, 5625–5628.
- (76) Shapovalov, V. L.; Möhwald, H.; Konovalov, O. V.; Knecht, V. Negligible water surface charge determined using Kelvin probe and total reflection X-ray fluorescence techniques. *Phys. Chem. Chem. Phys.* **2013**, *15*, 13991–13998.
- (77) Uematsu, Y.; Bonthuis, D. J.; Netz, R. R. Impurity Effects at Hydrophobic Surfaces. *Curr. Opin. Electrochem.* **2019**, *13*, 166–173.
- (78) Ducker, W. A. Contact angle and stability of interfacial nanobubbles. *Langmuir* **2009**, *25*, 8907–8910.
- (79) Das, S.; Snoeijer, J. H.; Lohse, D. Effect of impurities in description of surface nanobubbles. *Phys. Rev. E* **2010**, *82*, 056310.

- (80) Nicolás, J. A.; Vega, J. M. A note on the effect of surface contamination in water wave damping. *J. Fluid Mech.* **2000**, *410*, 367–373.
- (81) Maali, A.; Boisgard, R.; Chraïbi, H.; Zhang, Z.; Kellay, H.; Würger, A. Viscoelastic drag forces and crossover from no-slip to slip boundary conditions for flow near air-water interfaces. *Phys. Rev. Lett.* **2017**, *118*, 084501.
- (82) Arangalage, M.; Li, X.; Lequeux, F.; Talini, L. Dual Marangoni effects and detection of traces of surfactants. *Soft Matter* **2018**, *14*, 3378–3386.